Resonant soft x-ray scattering from stepped surfaces of $SrTiO_3$

2012 J. Phys.: Condens. Matter 24 035501

(http://iopscience.iop.org/0953-8984/24/3/035501)

IOP PUBLISHING JOURNAL OF PHYSICS: CONDENSED MATTER

J. Phys.: Condens. Matter **24** (2012) 035501 (9pp) doi:10.1088/0953-8984/24/3/035501

Resonant soft x-ray scattering from stepped surfaces of $SrTiO_3$

J Schlappa[1,2], C F Chang[1,3], Z Hu[1,3], E Schierle[2,4], H Ott[1,6], E Weschke[2,4], G Kaindl[4], M Huijben[5], G Rijnders[5], D H A Blank[5], L H Tjeng[1,3] and C Schüßler-Langeheine[1,2]

[1] II. Physikalisches Institut, Universität zu Köln, Zülpicher Str. 77, D-50937 Köln, Germany
[2] Helmholtz-Zentrum Berlin für Materialien und Energie GmbH, Albert-Einstein-Str. 15, 12489 Berlin, Germany
[3] Max Planck Institute for Chemical Physics of Solids, Nöthnitzer Str. 40, 01187 Dresden, Germany
[4] Institut für Experimentalphysik, Freie Universität Berlin, Arnimallee 14, D-14195 Berlin, Germany
[5] Faculty of Science and Technology and MESA+ Institute for Nanotechnology, University of Twente, Enschede, The Netherlands

E-mail: justine.schlappa@helmholtz-berlin.de

Received 2 February 2011, in final form 23 September 2011
Published 19 December 2011
Online at stacks.iop.org/JPhysCM/24/035501

Abstract
We studied the resonant diffraction signal from stepped surfaces of $SrTiO_3$ at the Ti 2p → 3d ($L_{2,3}$) resonance in comparison with x-ray absorption (XAS) and specular reflectivity data. The steps on the surface form an artificial superstructure suitable as a model system for resonant soft x-ray diffraction. A small step density on the surface is sufficient to produce a well defined diffraction peak. We determined the optical parameters of the sample across the resonance and found that the differences between the energy dependence of the x-ray absorption signal, the specular reflectivity and the step-related peak reflect the different quantities probed in these signals. When recorded at low incidence or detection angles, XAS and specular reflectivity spectra are strongly distorted by the changes of the angle of total reflection with energy. The resonant diffraction spectrum is less affected and can be used as a spectroscopic probe even in less favorable geometries.

1. Introduction

Resonant x-ray scattering in the soft x-ray range (RSXS) combines a high spectroscopic sensitivity with momentum resolution. It has very successfully been applied for many years to the study of mainly magnetic metal films and multilayers [1–13]. A more recent development is the application of RSXS to study phenomena such as charge and orbital order, as they are found in many correlated transition metal oxide systems [14]. Corresponding RSXS experimental results have been published in the last years from manganese systems [15–27], magnetite [28, 29], nickelates [30–32], cuprates [33–42] and ruthenates [43–45].

In 3d metal materials, the 2p → 3d excitation consists of rather broad resonance lines, reflecting the de-localized band-like character of the states. This is quite different from correlated transition metal oxides, in which the 2p → 3d excitation leads to local, excitonic states. Consequently the resonances here consist of a multiplet of fairly sharp resonance lines. Spatial modulations of the electronic state related to, e.g., charge ordering are reflected in different resonance multiplets for different lattice sites. They differ in the positions and intensities of the multiplet lines.

From the experiments on magnetic films and multilayers it is known that the resonances in the soft x-ray range are very strong and that x-ray optical effects have a huge influence on the observed signal. The change of the real part of the scattering tensor across resonance is not negligible and can dominate the specular reflectivity at low scattering angles, not only for the metal systems [1–13, 46] but also for semiconductors [47] and oxide thin films [48]. The question is now how these x-ray optical effects influence the resonant

[6] Present address: Shell Global Solutions International BV, Kesslerpark 1, 2288 GS, Rijswijk, The Netherlands.

soft x-ray scattering or diffraction signal from correlated transition metal oxide materials, which show very sharp multiplet structures.

It is hence a little unfortunate that for the case of oxides RSXS has so far been essentially applied to interesting but complex materials only. This is a consequence of the rather long photon wavelengths in the soft x-ray range. A suitable reference for an RSXD experiment requires sample periodicities in the nanometer range. For metals, multilayers are suitable samples for diffraction experiments. For oxides, this approach is problematic, since oxide multilayers turn out to have fairly complex electronic properties at the interfaces [23, 41].

Here we present a suitable simple model system to study soft x-ray optical effects for a typical transition metal oxide: stepped surfaces of single crystalline $SrTiO_3$. The system is electronically and structurally simple. The structure is cubic perovskite and because of the empty 3d shell of the Ti ions no electron-correlation effects need to be considered. In order to match the rather long photon wavelengths at the Ti 2p → 3d ($L_{2,3}$) resonance, we used the steps on vicinal surfaces as artificial superstructures with period lengths between about 20 and 70 nm. Samples with such surfaces allow us to study the diffraction signal caused by the steps, the specular reflectivity, and the x-ray absorption spectroscopy (XAS) signal and to compare these. One question that can be addressed with such a model is how sensitive RSXD is, i.e., what concentration of scatterers can be detected. As known for metals the optical parameters change strongly across a resonance in the soft x-ray range such that refraction effects matter. For the model system we could study how these x-ray optical effects affect the observed resonance data.

The rest of this contribution is organized as follows. Section 2 describes the sample system, section 3 the experimental setup, section 4 the experimental results from a stepped surface at large incidence and diffraction angles, section 5 the optical parameters of Ti in $SrTiO_3$ and section 6 how the different signals are affected by x-ray optical effects at different angles. In section 7 the results are summarized.

2. $SrTiO_3$

$SrTiO_3$ is a particularly appropriate system for model studies, because of its simple electronic and crystalline structure. The formal valence of the ions in this compound is Sr^{2+} ($5s^0$), Ti^{4+} ($3d^0$) and O^{2-} ($2p^6$), meaning that the electron shells of all ions are either fully occupied or empty in the ground state. Therefore it is a band insulator and possesses no magnetic moments. The crystal structure at room temperature is cubic perovskite (space group $Pm\bar{3}m$), with a lattice constant of 3.905 Å. The Ti ions are therefore embedded in an octahedral crystal field, generated by the neighboring oxygen ions. Due to this symmetry, the optical properties of the Ti ions are isotropic, which means independent of the polarization direction of the scattered light.

At energies around the Ti $L_{2,3}$ edge (∼460 eV) the optical properties of the compound are totally dominated by the dipole allowed Ti 2p → 3d transition. The Ti^{4+} ions are excited from the $2p^63d^0$ to a $2p^53d^1$ multiplet state, under the formation of a bound excitonic state between the core hole and the excited electron. Therefore this process can be well described in terms of a local picture, assuming that the electron is localized at the TiO_6 cluster. The absorption spectra of d^0 systems in O_h symmetry at transition metal $L_{2,3}$ edges have been extensively studied and modeled by de Groot *et al* [49], applying atomic multiplet calculations including crystal-field interactions. The spectra can be described by the $2p^53d^1$ multiplet, which consists of seven visible lines (see XAS curve in figure 1). The four most intense are split into two groups, due to the spin–orbit coupling of the core hole, such that the two at lower energies belong to the L_3 edge, whereas the other two to the L_2 edge. The splitting within each group is mainly determined by the crystal field splitting of the O_h symmetry, $10Dq$. Two of the weaker lines are on the low-energy side of the spectrum, the third in between the two L_3 main lines. They are due to the Coulomb and exchange interactions within the multiplet.

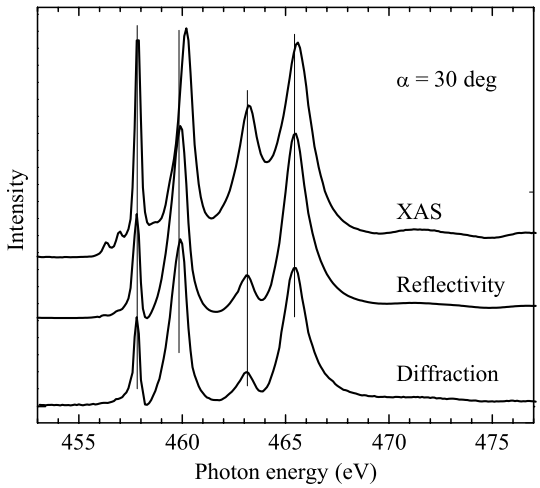

Figure 1. Energy dependence of the x-ray absorption (XAS), reflectivity and diffraction signal across the Ti $L_{2,3}$ edge for a 0.3°-inclined $SrTiO_3$ sample. The vertical lines denote the positions of the major peaks in the diffraction spectrum.

3. Experimental details

Samples with stepped surfaces were prepared at the University of Twente, The Netherlands. In order to obtain a well defined TiO_2-terminated surface, the $SrTiO_3$ single crystals were etched in buffered HF and subsequently annealed in oxygen [50]. The samples had the form of square plates with an edge length of 10 mm and a thickness of 0.5 or 1 mm. The surface orientation was essentially (001). For the diffraction experiments we used samples with miscut angles, i.e., the difference between the averaged surface and the surface of one terrace on the surface, of about 0.3 and about 1°. This corresponds to a terrace width of 70 and 20 nm, respectively. The samples were characterized by atomic force microscopy (AFM) and x-ray absorption spectroscopy (XAS). Figure 2 shows AFM data of one of the samples. The steps are equally spaced, though slightly wavy, leading to a regular stripe-like

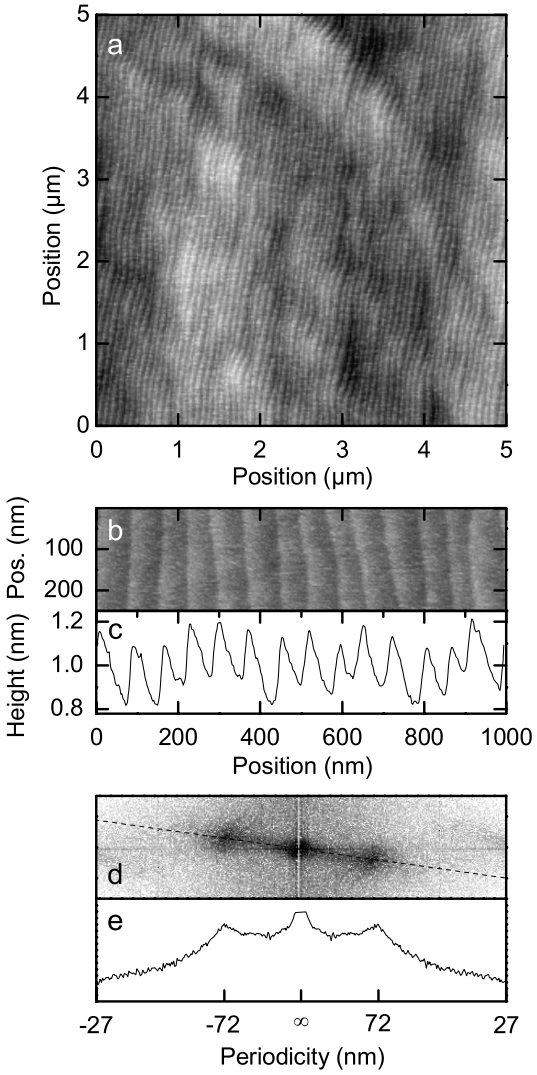

Figure 2. Atomic force microscopy (AFM) data from one of the used stepped $SrTiO_3$ surfaces with a miscut angle of ≈0.3°: the field of vision of 5 × 5 μm^2 (a) and 250 × 1000 nm^2 in the enlarged view (b). (c) The height profile of the surface; (d) the Fourier transform of the AFM image in (b); (e) a line cut along the dotted line in (d). For the scattering experiment the stepped samples were mounted such that the edge of the steps was oriented perpendicular to the scattering plane.

surface structure. The edges of the terraces are almost parallel to the sample edge, which has the direction [100]. The Fourier transform in figure 2(e) demonstrates that the disorder of the steps suppresses the higher-order peaks.

For the scattering experiment the stepped samples were mounted such that the edge of the steps was oriented perpendicular to the scattering plane and the incident beam was pointing toward the steps (see figure 3). After transfer into UHV, the samples were annealed to 300 °C in an oxygen atmosphere of 5 × 10^{-5} mbar for 30 min, to desorb gas particles adhering to the surface.

The experiments were performed at the UE52-SGM1 beamline at BESSY using the UHV soft x-ray diffractometer designed at the FU Berlin. The scattering geometry was horizontal with the light linearly polarized parallel to the

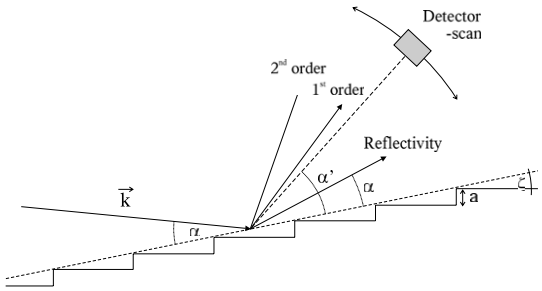

Figure 3. Schematic diagrams of the scattering geometry for diffraction from a stepped surface. $\vec{k}$ denotes the wavevector of the incoming photon, α the angle between $\vec{k}$ and the averaged sample surface, which is at an angle ζ with the surface of one of the terraces, α' the angle between the averaged surface and the detector and a the lattice constant of $SrTiO_3$.

scattering plane (π direction). The photons were detected using a photo-diode mounted behind a rectangular slit. For the energy scans from the step peaks the detector position and the photon energy was scanned simultaneously in order to stay on the diffraction peak. The detector acceptance was chosen such that the whole peak is detected. The energy dependence of the background below the peak was measured separately, with the detector angles shifted by 3°, and was subtracted from the peak spectra. The x-ray absorption spectra were obtained from the total electron yield signal recorded with a Channeltron electron detector.

4. Diffraction data

A regular arrangement of steps on a surface has the properties of a reflection grating. When the height of these steps is equal to the lattice parameter a and ζ is the miscut angle, the width of the terraces will be equal to $a/\tan\zeta$. A diffraction signal can be observed when the following condition is fulfilled:

$$\frac{a}{\tan\zeta}(\cos\alpha - \cos\alpha') = m\lambda \qquad (1)$$

with the integer m giving the diffraction order. The angles of incidence and diffraction, α and α', are expressed here with respect to the averaged surface (figure 3), λ is the x-ray wavelength, which is for the Ti $L_{2,3}$ resonance about 27 Å. For a two-dimensional superstructure the reciprocal lattice consists of one-dimensional rods, rather than of a three-dimensional array of points. If the wavelength is shorter than the terrace width, the diffraction condition of equation (1) can be fulfilled for any chosen angle of incidence. For a particular angle of incidence several reflections can be observed, as illustrated in figure 3, one belonging to the specular reflectivity ($m = 0$, $\alpha' = \alpha$) and others to diffraction from the terraces. These reflections can be probed, e.g. by scanning the detector angle α'.

In order to test the signal strength, we first performed an experiment far from resonance. Figure 4 shows an off-resonance scan measured from a 1.09°-inclined sample by changing the detector angle. The angle of incidence was kept at 5° and the photon energy was 900 eV, lying far

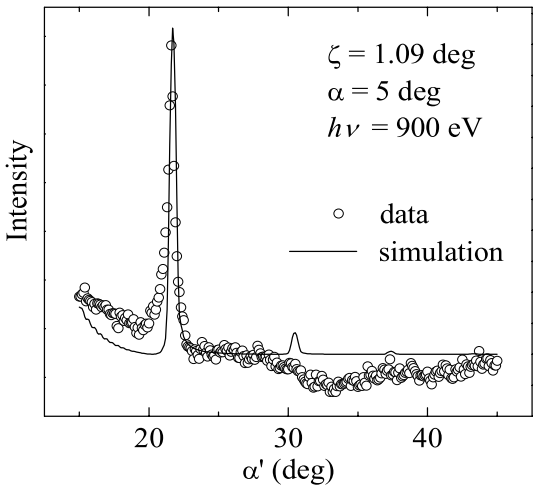

Figure 4. Detector-angle scan across the diffraction peaks from a stepped 1.09°-inclined $SrTiO_3$ sample, recorded off resonance.

above the Ti resonance. The symbols in the diagram represent experimental data whereas the solid line is a simulation using a simple kinematical model of scattering from steps. The data show a pronounced maximum around 21.7°, which is the position for the first-order reflection. The observation of this signal clearly demonstrates the suitability of this model system for soft x-ray diffraction. For the given photon energy and scattering geometry we can estimate the volume of Ti ions at step edges to be about 3×10^{-4} of the total scattering volume, V, given by [51]

$$V = \frac{S\Lambda}{1 + \sin(\alpha)/\sin(\alpha')} \tag{2}$$

with S being the photon beam cross-section of $100 \times 100\ \mu m^2$ and Λ the photon mean free path [52]. The clear signal observed even off resonance shows that diffraction using soft x-ray energies is sensitive enough to study even very 'dilute' systems.

The second-order peak cannot be resolved from the background signal. Apparently its intensity is lower than expected for an ideal system, probably due to the waviness of the step edges. The angular width of the measured first-order diffraction peak shows that the widths of the terraces on the surface vary around the average value. In the simulation a Gaussian distribution of widths around $a/\tan\zeta$ was considered. The increase of background toward low detector angles is due to the tail of the reflectivity.

We note that, compared to a line grating used nowadays in soft x-ray beam lines, the intensity in the first-order peak is very low. The stepped surface studied here has a 'line density' of 50 000 mm^{-1}, which is higher by one to two orders of magnitude than that of common x-ray gratings. The fact that the signal observed here is rather weak is partially due to low reflectance $SrTiO_3$ in this energy range as compared to the metal coating of the x-ray grating and partially due to the imperfections in the step pattern and surface roughness.

When the photon energy is tuned to the Ti L_2- or L_3-edge, the diffraction signal increases considerably by about one order of magnitude. The intensity of the diffraction signal varies strongly across the resonance edge, as energy is changed. Figure 1 shows an energy scan of the diffraction signal (lower curve), compared with the x-ray absorption (XAS) and reflectivity spectrum for the same energy range. All spectra were taken from a 0.31°-inclined sample at 30°incidence angle. For the step peak the detector was around 34°. The diffraction and reflectivity spectra look almost identical. They show the four main resonance peaks discussed above, which are also present in the absorption spectrum. The relative intensities of the main peaks in the absorption spectrum and the scattering data are different, with the weak lines more pronounced in the XAS data than in the diffraction and reflectivity data. In fact, it is not expected for the absorption spectrum to look like the diffraction or reflectivity signal since XAS is probing only the imaginary part of the scattering amplitude, whereas the other two signals are determined by the squared modulus of the sum of the real and imaginary part of the scattering amplitude.

For a single harmonic oscillator the absorption spectrum is a Lorentzian [53] of width Γ and intensity A. The scattered intensity determined by the norm squared of the real and the imaginary part is (ignoring the interference with non-resonant contributions to the scattering amplitude) again a Lorentzian of the same width but with an intensity proportional to A^2/Γ. This leads to a general enhancement of strong and narrow resonance lines in the scattered signal. For the case of several overlapping resonances, as we have them here, the interference between the different oscillators also matters. In fact, in the reflectivity and diffraction spectra, the peak maxima of the major peaks except for that at the lowest photon energy are shifted by up to 0.3 eV toward lower energies with respect to the XAS data. In order to check whether the observed energy shift is indeed an interference effect, we determined the optical parameters of $SrTiO_3$.

5. Optical parameters

Off resonance the index of refraction is tabulated [52], but these tables are not accurate enough near resonances. Optical parameters near resonance energies can be determined, e.g., from measurements of the absorption cross-section μ, which is proportional to the imaginary part of the scattering cross-section: $\beta = -\lambda\mu/4\pi$ [53]. δ is then determined via Kramers–Kronig transformation of β [7, 8, 11]. The precision of this approach depends mainly on the accuracy with which the absorption cross-section can be obtained, and is highest in a transmission experiment [11], while total electron yield measurements suffer to some extent from saturation effects. Since transmission experiments are difficult to perform for a bulk sample, we chose to determine the optical parameters from reflectivity measurements [3, 6, 47] from a flat sample of $SrTiO_3$ as a function of photon energy around the Ti $L_{2,3}$ resonance using π-polarized light.

The intensity of the reflectivity signal is described by Fresnel equations, which are functions of the angle of incidence and the refraction index [54]. For the interface

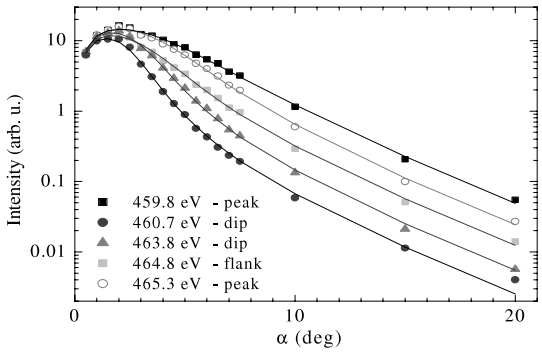

Figure 5. Reflectivity curves (symbols) as a function of the angle of incidence α for different characteristic photon energies on a logarithmic scale; the solid lines are fits applying the Fresnel equation and the footprint effect at low incidence angles.

between vacuum and a medium with refractive index n, the amplitude of the reflected wave for π polarization, E_π, is

$$E_\pi(\alpha, n) = E_0 \frac{n^2 \sin\alpha - \sqrt{n^2 - \cos^2\alpha}}{n^2 \sin\alpha + \sqrt{n^2 - \cos^2\alpha}} \qquad (3)$$

with E_0 being the intensity of the incident wave. Therefore, knowing the dependence of the signal on the angle of incidence α, the index of refraction n can be obtained experimentally, and consequently, according to $n = 1 - \delta + i\beta$, also the optical constants δ and β.

Figure 5 shows reflectivity data for selected energies (symbols), together with the result of a least square fit (lines). The intensity of the signal decreases approximately exponentially with larger angles of incidence. At low angles total external reflection occurs, leading to the maximum around 2°. The decrease of signal for $\alpha < 2°$ seen in the data is due to the fact that for very small incidence angles the footprint of the x-ray beam on the sample surface becomes larger than the sample itself, leading to a loss of intensity. In this region the intensity of the light falling on the sample is proportional to $(x \sin\alpha)/b$, where x is the sample width and b the beam-width in the scattering plane.

The data were analyzed using the Fresnel equation for π-polarized light equation (3) and a Debye–Waller-like damping to account for the sample roughness of 3 Å [53]. The analysis of reflectivity data works best when the reflectivity curve is structured like that from a multilayer [3, 6]. For flat samples the problem occurs that for large negative values of δ (indicated in figure 6 by the gray points) the shape of the reflectivity curve depends only very weakly on the value of n for a wide range of (δ, β) sets [55]. The fit does not hence converge in this region. Except for the main line at the lowest energy, this convergence problem does not affect the peak values of β but only the low-energy side of the resonance lines. We could therefore use the shape of the XAS data in this energy region to interpolate the β values without being too much affected by saturation effects. These interpolated values were then used in the fit to determine δ.

The thus obtained optical constants δ and β are shown in figure 6, together with the absorption spectrum (XAS) at 30° incidence angle (upper curve). The error bars denote the

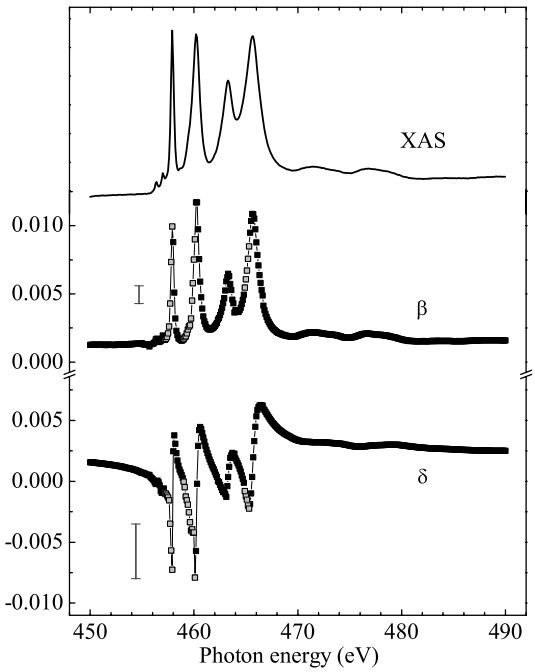

Figure 6. Optical parameters δ and β together with the absorption spectrum (XAS) at 30° of incidence. The error bars indicate the uncertainty for the gray marked points. For the black marked points the error margins are around 10%.

maximum uncertainty for the data points denoted by gray symbols. For values shown with black symbols the uncertainty for δ amounts to 10%, whereas for β it is a little bit smaller. Above the resonance at 490 eV, δ is approximately 2.5×10^{-3} and β is 1.6×10^{-3}, which agrees very well with the tabulated x-ray data [52], giving for this energy 2.3×10^{-3} and 1.5×10^{-3}, respectively (using a mass density, ρ_a of 5 g cm^{-3} for the sample).

Across the resonance the optical constants are strongly energy dependent. While β resembles the absorption spectrum, reaching peak values at each resonance—with the maximum of 12×10^{-3} at 460.25 eV, δ behaves similarly to the negative derivative of β. δ changes sign each time a strong absorption peak is crossed; coming from the low-energy side it decreases steadily, reaching a negative-signed minimum just before the absorption peak; directly above the absorption maximum it increases steeply toward a positive-signed maximum, crossing the zero line exactly at the resonance position, and decreases again more slowly afterward, crossing the zero line in the vicinity of a local β minimum. The largest absolute value that δ reaches is negative signed and amounts to -8×10^{-3} at 460.1 eV.

6. Optical effects in the spectra

In figure 7 we present the result of a simulation of the diffraction-peak spectrum from figure 1 using the optical parameters. The dashed curve was calculated from

$$I = |f_0 + f' + if''|^2 = \left| \frac{2\pi}{\lambda^2 \rho_a r_0} (\delta - i\beta) \right|^2 \qquad (4)$$

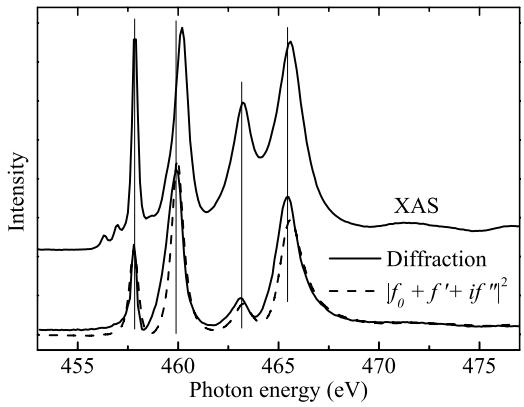

Figure 7. XAS and diffraction data from figure 1 with the result of a simulation of the diffraction spectrum using the optical parameters from figure 6 (dashed line).

and was broadened by 300 meV to account for the fact that the energy resolution for the XAS spectrum was chosen to be higher than for the diffraction spectrum ($r_0 \approx 2.82 \times 10^{-5}$ Å is the classical electron radius, $\frac{2\pi}{\lambda^2 \rho_a r_0} \approx 18\,410$ at 462 eV). The simulated curve describes the experimental curve fairly well, including the relative intensities. In particular, the shifted energy position of the second sharp maximum is essentially reproduced. Even though the agreement is less satisfactory for the L_2 part of the spectrum, this simple purely optical simulation indicates that the observed spectral differences between XAS and scattering data are mainly the result of the different optical quantities probed in the different experiments.

While the data from figure 1 were recorded at large incidence and detection angles of 30°and 34°, at small angles the effect of refraction of the photons in the sample becomes more and more important.

How these changes affect the spectra is demonstrated in figure 8, where the corresponding signals are shown for two different surfaces and for different incidence angles $\alpha = 5°$, 10°, 20° and 30°. The corresponding detection angles α' varied around 16.5°, 18.5°, 25.5°and 34° for the 0.31°sample and around 30°, 31°, 36°and 42.5° for the 1.09° sample. Least affected by the variation of the incidence angle are the diffraction spectra for the 1.09° sample, for which the detector angles α' were largest. Changes are somewhat more present for the 0.31° sample diffraction spectra with smaller α'-values. The peak maxima shift toward higher energies and the background on the high-energy side of the spectrum rises, while the overall shape of the spectrum is conserved. Much more pronounced changes of the spectral shape are found for the reflectivity signal and they occur in the same way for both samples. For comparison the reflectivity signal of the 0.31 sample at 5° of incidence has also been plotted, as the dotted line in the right diagram of figure 8.

It is instructive to convert β and δ into more practical quantities: The changes of δ across resonance lead to fairly large variations of the angle of total reflection, α_c. The changes of β affect the photon mean free path Λ. Figure 9 shows these quantities in comparison with the XAS data across the Ti $L_{2,3}$ resonance in $SrTiO_3$. Λ and α_c can be directly obtained from the optical constants; $\Lambda = 1/\mu$ is the inverse of $4\pi\beta/\lambda$ and α_c is given by $\cos\alpha_c = \sqrt{1-\delta}$. The probing depth of an x-ray scattering experiment is given by $(\Lambda \sin\alpha')/(\sin\alpha \sin\alpha' + \sin^2\alpha)$, which for normal incidence and detection becomes $\Lambda/2$. Below and above the resonance energies Λ has values well above 100 nm, meaning that for not too small scattering angles the signal

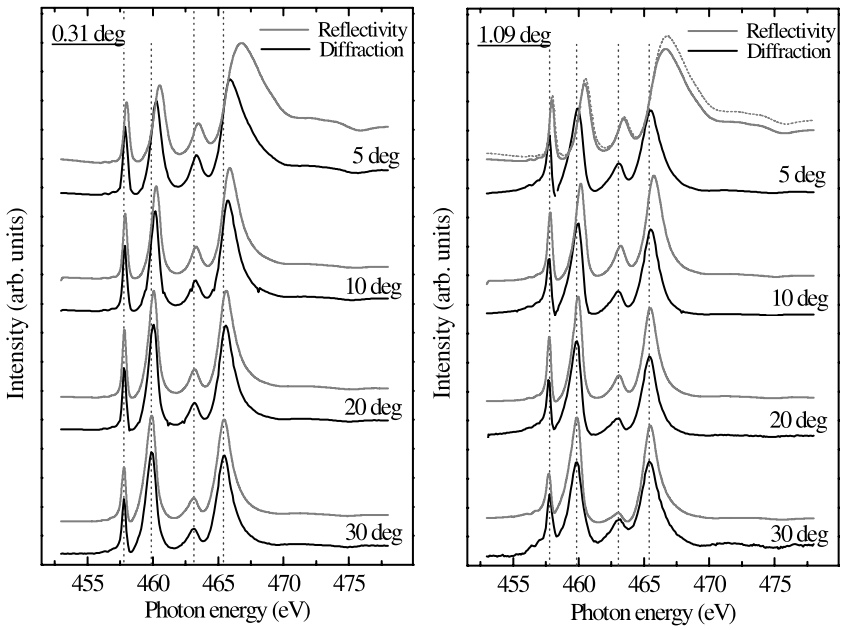

Figure 8. Reflectivity and diffraction data from 0.31°- (left) and 1.09°- (right) inclined samples for different incidence angles ($\alpha = 5$, 10, 20, 30). The dotted curve for $\alpha = 5$ on the right side is the reflectivity of the 0.31° sample plotted for comparison.

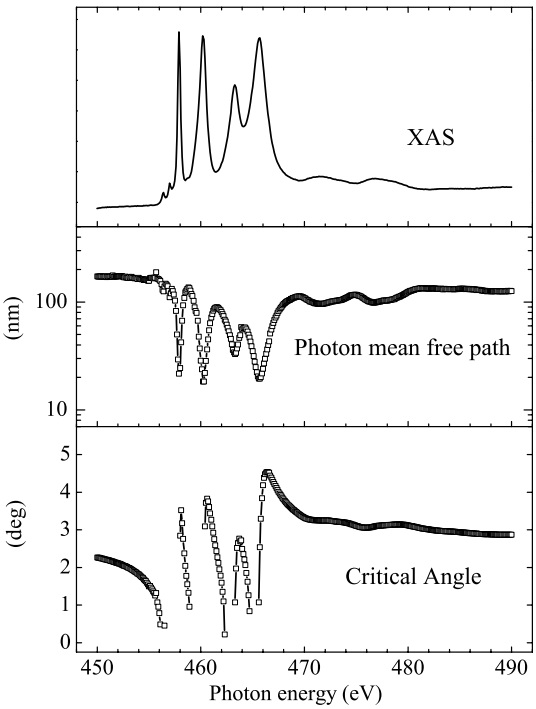

Figure 9. XAS spectrum (top), photon mean free path Λ on a logarithmic scale (middle) and critical angle α_c (bottom), the latter two obtained from the optical constants presented in figure 6.

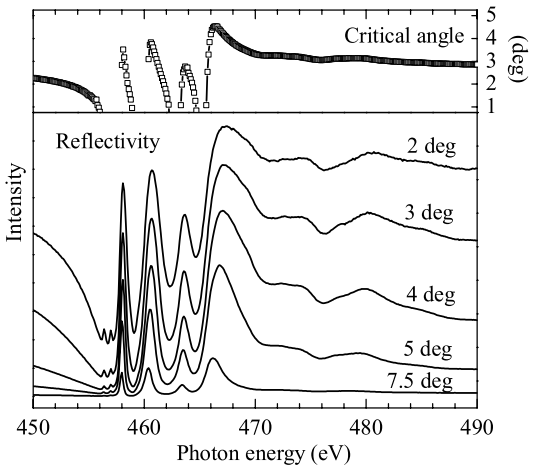

Figure 10. Reflectivity for low incidence angles of the flat $SrTiO_3$ sample (lower frame). The upper frame shows the critical angle calculated from δ.

is clearly bulk sensitive. At the resonance maxima the photon mean free path drops to 20 nm, which is moderately surface sensitive. Even at its minimum value Λ is one order of magnitude larger than the probing depth in typical surface-sensitive techniques involving low-energy electrons, such as photoelectron spectroscopy.

The critical angle varies across the resonance, approximately as $\sqrt{\delta}$. Outside resonance α_c has a value between 2° and 3°. Above each resonance maximum it reaches peak values, the highest being 4.5° for 478 eV photon energy on the high-energy side of the resonance spectrum. For energies just below each resonance maximum, where δ becomes negative, α_c is not defined and the effect of total external reflection disappears completely. The size and variation of α_c is similar to that observed, e.g., for iron metal [10]. The more structured resonance spectrum in the case of $SrTiO_3$ causes, however, a much more rapid variation of α_c with photon energy.

This rapid variation of α_c with energy will strongly affect reflectivity and absorption spectra measured at low incidence angles [48]. Figure 10 shows specular reflectivity data for α between 7.5° and 2°. The top diagram displays α_c for comparison. The reflectivity data are all plotted on the same scale. The curve measured at $\alpha = 7.5°$ resembles very much specular reflectivity for high incidence angles, but as the angle of incidence becomes smaller the shape of the spectra changes considerably. Approaching the critical angle, the positions of the main peaks shift toward higher energies and the relative intensities of the spectrum features change; the intensity outside resonance increases strongly in comparison to the main peaks and smaller features of the spectra become more visible. Comparison with the values of the critical angle α_c at energies where these changes are particularly strong makes it clear that these effects are caused by total reflection. As the incidence angle approaches α_c, the intensity of specular reflectivity increases strongly, e.g. at the position of the highest energy peak (466 eV) close to $\alpha = 5°$ and at the background below the resonance edge close to $\alpha = 3°$. When the incidence angle becomes smaller than the critical angle, the increase in intensity is reduced, because total reflection has already been reached.

The influence of α_c on the absorption spectra (XAS) is even more dramatic. Since only those photons that can penetrate the surface can be absorbed, a high reflectivity suppresses the XAS signal [48, 56]. This effect leads to a distortion of the spectra and dominates at low incidence angles the shape of the XAS spectra, which become the negative of the reflectivity spectra. This fact is most obvious for the data measured at 1.5° incidence in the center of figure 11 with minima in the absorption spectrum exactly at the positions of the maxima in the reflectivity signal. Well above the critical angle the two spectra look very similar (see 30° of incidence). These results show that the effect of total reflection indeed dominates both reflectivity and absorption spectra, for low incidence angles.

7. Summary

The stepped surface of a single crystal can work as an artificial two-dimensional superstructure, with a periodicity in the nanometre range, which can be used to produce diffraction peaks with soft x-rays. The signal is clearly visible, even for a step density smaller than 1/50 of the topmost layer and considerable disorder of the steps, and can be further amplified if energies corresponding to a resonance edge of the system are used. We investigated at the Ti $L_{2,3}$ resonance the first-order diffraction signal from stepped $SrTiO_3$ surfaces with a terrace width of 20 and 70 nm. The spectrum of the diffraction signal with energy resembles the spectrum for the specular reflectivity data. The x-ray absorption spectrum

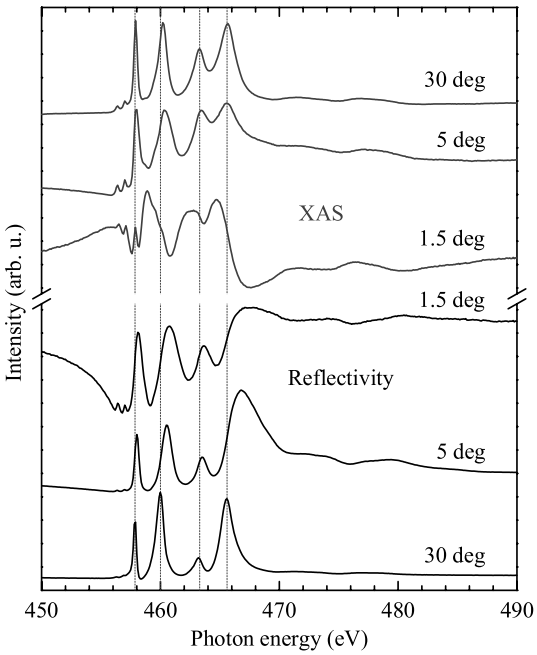

Figure 11. Comparison of XAS (top three curves) and reflectivity data for different angles of incidence ($\alpha = 30$, 5 and 1.5).

differs from both in the relative intensities of the spectral features and in the energy position of the peak maxima. We determined the optical parameters across resonances from specular reflectivity and found that the deviations in the spectral shape between XAS and scattering data reflect the different quantities probed in the different signals. The fact that the two scattering signals are probing the squared norm of the scattering cross-section leads to an enhancement of the stronger over the weaker spectral features in the scattering signals.

Changes of the optical sample properties across resonance distort the reflectivity and XAS spectra recorded at especially small incidence angles. This distortion is related to the change of the angle of total reflection with photon energy, which dominates the spectral shape of both signals at very small angles. The spectral shape of the resonant diffraction spectra from the step edges are less affected, mainly because even for small incidence angles the detection angles are comparably large; we only find small shifts in the energy of the resonance maxima. Therefore x-ray diffraction data can deliver spectroscopic information even in geometries which are less favorable for reflectivity measurements, due to e.g. grazing incidence angles.

Acknowledgments

We gratefully acknowledge the expert support and excellent working conditions at BESSY and skilful technical assistance by L Hamdan. The research in Köln was supported by the Deutsche Forschungsgemeinschaft through SFB 608. G R and D B acknowledge support from the Netherlands Organization for Scientific Research (NWO).

References

[1] Kao C, Hastings J B, Johnson E D, Siddons D P, Smith G C and Prinz G A 1990 *Phys. Rev. Lett.* **65** 373–6
[2] Kao C C *et al* 1994 *Phys. Rev.* B **50** 9599–602
[3] Tonnerre J M, Sève L, Raoux D, Soullié G, Rodmacq B and Wolfers P 1995 *Phys. Rev. Lett.* **75** 740–3
[4] Chen C T, Ydzerda Y U, Kao C C, Tjeng L H, Lin H J and Meigs G 1995 *Mater. Sci. Eng.* **B31** 49–56
[5] Chen C T, Ydzerda Y U, Kao C C, Tjeng L H, Lin H J and Meigs G 1995 *Mater. Res. Soc. Symp. Proc.* **375** 59–70
[6] Sève L, Tonnerre J M and Raoux D 1998 *J. Appl. Cryst.* **31** 700–7
[7] Sacchi M, Hague C F, Pasquali L, Mirone A, Mariot J M, Isberg P, Gullikson E M and Underwood J H 1998 *Phys. Rev. Lett.* **81** 1521–4
[8] Sacchi M and Mirone A 1998 *Phys. Rev.* B **57** 8408–15
[9] Schüßler-Langeheine C *et al* 2001 *J. Electron Spectrosc. Relat. Phenom.* **114–116** 953
[10] Kortright J B and Kim S K 2000 *Phys. Rev.* B **62** 12216–28
[11] Peters J F, Miguel J, de Vries M A, Toulemonde O M, Goedkoop J B, Dhesi S S and Brookes N B 2004 *Phys. Rev.* B **70** 224417
[12] Ott H, Schüßler-Langeheine C, Schierle E, Grigoriev A Y, Leiner V, Zabel H, Kaindl G and Weschke E 2006 *Phys. Rev.* B **74** 094412(R)
[13] Ott H, Schüßler-Langeheine C, Schierle E, Kaindl G and Weschke E 2006 *Appl. Phys. Lett.* **88** 212507
[14] Imada M, Fujimori A and Tokura Y 1998 *Rev. Mod. Phys.* **70** 1039–263
[15] Wilkins S B, Hatton P D, Roper M D, Prabhakaran D and Boothroyd A T 2003 *Phys. Rev. Lett.* **90** 187201
[16] Wilkins S B, Spencer P D, Hatton P D, Collins S P, Roper M D, Prabhakaran D and Boothroyd A T 2003 *Phys. Rev. Lett.* **91** 167205
[17] Dhesi S S *et al* 2004 *Phys. Rev. Lett.* **92** 056403
[18] Thomas K J *et al* 2004 *Phys. Rev. Lett.* **92** 237204
[19] Wilkins S B, Stojic N, Beale T A W, Binggeli N, Castleton C W M, Bencok P, Prabhakaran D, Boothroyd A T, Hatton P D and Altarelli M 2005 *Phys. Rev.* B **71** 245102
[20] Staub U, Scagnoli V, Mulders A M, Katsumata K, Honda Z, Grimmer H, Horisberger M and Tonnerre J M 2005 *Phys. Rev.* B **71** 214421
[21] Wilkins S B, Stojic N, Beale T A W, Binggeli N, Hatton P D, Bencok P, Stanescu S, Mitchell J F, Abbamonte P and Altarelli M 2006 *J. Phys.: Condens. Matter* **18** L323–9
[22] Staub U, Scagnoli V, Mulders A M, Janousch M, Honda Z and Tonnerre J M 2006 *Europhys. Lett.* **76** 926–32
[23] Smadici Ş, Abbamonte P, Bhattacharya A, Zhai X, Jiang B, Rusydi A, Eckstein J N, Bader S D and Zuo J M 2007 *Phys. Rev. Lett.* **99** 196404
[24] Grenier S, Kiryukhin V, Cheong S W, Kim B G, Hill J P, Thomas K J, Tonnerre J M, Joly Y, Staub U and Scagnoli V 2007 *Phys. Rev.* B **75** 085101
[25] Grenier S *et al* 2007 *Phys. Rev. Lett.* **99** 206403
[26] Bodenthin Y, Staub U, García-Fernández M, Janoschek M, Schlappa J, Golovenchits E I, Sanina V A and Lushnikov S G 2008 *Phys. Rev. Lett.* **100** 027201
[27] García-Fernández M, Staub U, Bodenthin Y, Lawrence S M, Mulders A M, Buckley C E, Weyeneth S, Pomjakushina E and Conder K 2008 *Phys. Rev.* B **77** 060402(R)
[28] Huang D J *et al* 2006 *Phys. Rev. Lett.* **96** 096401
[29] Schlappa J *et al* 2008 *Phys. Rev. Lett.* **100** 026406
[30] Schüßler-Langeheine C *et al* 2005 *Phys. Rev. Lett.* **95** 156402
[31] Scagnoli V, Staub U, Mulders A M, Janousch M, Meijer G I, Hammerl G, Tonnerre J M and Stojic N 2006 *Phys. Rev.* B **73** 100409

[32] Staub U, García-Fernández M, Mulders A M, Bodenthin Y, Martínez-Lope M J and Alonso J A 2007 *J. Phys. Condens. Matter* **19** 092201
[33] Abbamonte P, Venema L, Rusydi A, Sawatzky G A, Logvenov G and Bozovic I 2002 *Science* **297** 581–4
[34] Abbamonte P, Blumberg G, Rusydi A, Gozar A, Evans P G, Siegrist T, Venema L, Eisaki H, Isaacs E D and Sawatzky G A 2004 *Nature* **431** 1078–81
[35] Abbamonte P, Rusydi A, Smadici S, Gu G D, Sawatzky G A and Feng D L 2005 *Nature Phys.* **1** 155–8
[36] Rusydi A, Abbamonte P, Eisaki H, Fujimaki Y, Blumberg G, Uchida S and Sawatzky G A 2006 *Phys. Rev. Lett.* **97** 016403
[37] Rusydi A, Berciu M, Abbamonte P, Smadici S, Eisaki H, Fujimaki Y, Uchida S, Rübhausen M and Sawatzky G A 2007 *Phys. Rev.* B **75** 104510
[38] Smadici Ş, Abbamonte P, Taguchi M, Kohsaka Y, Sasagawa T, Azuma M, Takano M and Takagi H 2007 *Phys. Rev.* B **75** 075104
[39] Rusydi A, Abbamonte P, Eisaki H, Fujimaki Y, Smadici S, Motoyama N, Uchida S, Kim Y J, Rübhausen M and Sawatzky G A 2008 *Phys. Rev. Lett.* **100** 036403
[40] Rusydi A *et al* 2008 *Appl. Phys. Lett.* **92** 262506
[41] Smadici S, Lee J C T, Wang S, Abbamonte P, Logvenov G, Gozar A, Deville Cavellin C and Bozovic I 2009 *Phys. Rev. Lett.* **102** 107004
[42] Fink J *et al* 2009 *Phys. Rev.* B **79** 100502
[43] Zegkinoglou I *et al* 2005 *Phys. Rev. Lett.* **95** 136401
[44] Bohnenbuck B *et al* 2008 *Phys. Rev.* B **77** 224412
[45] Bohnenbuck B *et al* 2009 *Phys. Rev. Lett.* **102** 037205
[46] André J M, Barchewitz R, Maquet A and Marmoret R 1984 *Phys. Rev.* B **29** 6576–85
[47] André J M, Maquet A and Barchewitz R 1982 *Phys. Rev.* B **25** 5671–9
[48] Alders D, Hibma T, Sawatzky G A, Cheung K C, van Dorssen G E, Roper M D, Padmore H A, van der Laan G, Vogel J and Sacchi M 1997 *J. Appl. Phys.* **82** 3120–4
[49] de Groot F M F, Fuggle J C, Thole B T and Sawatzky G A 1990 *Phys. Rev.* B **41** 928–37
[50] Koster G, Kropman B L, Rijnders G, Blank D H A and Rogolle H 1998 *Appl. Phys. Lett.* **73** 2920
[51] Guinier A 1994 *X-ray Diffraction in Crystals, Imperfect Crystals, and Amorphous Bodies* (New York: Dover)
[52] Henke B L, Gullikson E M and Davis J 1993 *At. Data Nucl. Data Tables* **54** 181–342
[53] Als-Nielsen J and McMorrow D 2001 *Elements of Modern X-ray Physics* (New York: Wiley)
[54] Jackson J D 1962 *Classical Electrodynamics* (New York: Wiley)
[55] Soufli R and Gullikson E M 1997 *Appl. Opt.* **36** 5499–507
[56] van der Laan G and Thole B T 1988 *J. Electron Spectrosc. Relat. Phenom.* **46** 123–9